

ARTICLE

Geochemical evidence for the application of nanoparticulate colloidal silica gel for in-situ containment of legacy nuclear wastes

Received 00th January 20xx,
Accepted 00th January 20xx

Pieter Bots,^{*a} Joanna C. Renshaw,^a Timothy E. Payne,^b M. Josick Comarmond,^b Alexandra E.P. Schellenger,^a Matteo Pedrotti,^a Eleonora Cali^c and Rebecca J. Lunn^a

DOI: 10.1039/x0xx00000x

Colloidal silica is a nanoparticulate material that could have a transformative effect on environmental risk management at nuclear legacy sites through their use in in-situ installation of injectable hydraulic barriers. In order to utilize such nanoparticulate material as a barrier, we require detailed understanding of its impact on the geochemistry of radionuclides in the environment (e.g. fission products such as Sr and Cs). Here we show, through combining leaching experiments with XAS analyses, that colloidal silica induces several competing effects on the mobility of Sr and Cs. First, cations within the colloidal silica gel compete with Sr and Cs for surface complexation sites. Second, an increased number of surface complexation sites is provided by the silica nanoparticles and finally, the elevated pH within the colloidal silica increases the surface complexation to clay minerals and the silica nanoparticles. XAS analyses show that Sr and Cs complex predominantly with the clay mineral phases in the soil through inner-sphere surface complexes (Sr) and through complexation on the clay basal surfaces at Si vacancy sites (Cs). For binary soil – colloidal silica gel systems, a fraction of the Sr and Cs complexes with the amorphous silica-like surfaces through the formation of outer-sphere surface complexes. Importantly, the net effect of nanoparticulate colloidal silica gel is to increase the retention of Sr and Cs, when compared to untreated soil and waste materials. Our research opens the door to applications of colloidal silica gel to form barriers within risk management strategies at legacy nuclear sites.

Environmental Significance

Nuclear legacy sites containing radioactive wastes and contamination exist worldwide and their long-term management, remediation and decommissioning are subjects of public concern. To ensure long-term safety, risk mitigation strategies such as hydraulic barriers are essential. Traditional barrier materials (including cement and bentonite) require high-pressure injection or excavation, neither of which is desirable at contaminated nuclear sites. Because nanoparticulate colloidal silica gel can be used with minimal land disturbance, it is a promising alternative barrier material. Prior to realizing the potential of such nanoparticulate materials, it is essential to understand their impacts on risk determining radionuclides and other contaminants. The presented research reveals the mechanisms through which colloidal silica gel inhibits the migration of Sr and Cs at legacy nuclear sites.

Introduction

Nuclear power at present provides approximately 10% of the world's electricity requirements. However, over six decades of civil nuclear power generation, and a longer history of research and military nuclear activities, have led to significant quantities of radioactive wastes¹ and contaminated sites.² Contaminated legacy sites include Hanford, WA, USA,^{3, 4} Savannah River, SC, USA,⁵ Sellafield, Cumbria, UK^{6, 7} and the Little Forest Legacy Site (LFLS), NSW, Australia.⁸ Contamination at such sites can be a result of historical containment strategies, e.g. shallow burial in unlined trenches,² or from the deterioration of containment structures that are now beyond their designed lifetimes.^{3, 7} Radioactive contamination (e.g. Sr, Cs, Tc, U and Pu) has been detected at many such legacy waste sites⁴⁻¹⁰ indicating a potential for further contamination during decommissioning activities.

Long-term options to minimize the risks of such legacy sites can include the installation of subsurface hydraulic or reactive barriers to prevent contaminant transport.¹¹⁻¹³ Retrofitting such engineering options near-surface is problematic, as traditional barriers use bentonite slurries or cementitious materials and their installation causes significant soil disturbance and generates contaminated soil wastes for subsequent disposal.¹¹ Nanotechnology could play a pivotal role in minimizing risks at nuclear legacy sites;¹⁴ colloidal silica is an alkaline suspension of silica nanoparticles that forms a very low permeability hydrogel

^a Department of Civil and Environmental Engineering, University of Strathclyde, Glasgow, G1 1XJ, United Kingdom. E-mail: pieter.bots@strath.ac.uk

^b Australian Nuclear Science and Technology Organisation, Lucas Heights, NSW 2234, Australia.

^c Department of Materials, Imperial College London, London, SW7 2AZ, United Kingdom.

† Electronic Supplementary Information (ESI) available: detailed experimental methods and the respective data treatment and a brief discussion of the aqueous results from the leaching experiments to produce XAS samples. See DOI: 10.1039/x0xx00000x

when destabilized by cations in a saline solution. It is promising as an alternative barrier material due to its initial low viscosity, chemical inertness, and negligible toxicity.^{12, 13} These properties could make colloidal silica gel an ideal material for in-situ environmental containment. To realize the potential of nanoparticulate colloidal silica for legacy nuclear sites, it is first necessary to understand such nanomaterials¹⁵ and their respective impacts on the mobility of contaminants,¹⁴ specifically radionuclides.^{15, 16}

Radionuclides are produced during the generation of nuclear energy and are present within wastes and as soil and groundwater contaminants. The fission products Cs and Sr are common contaminants at nuclear legacy sites^{4-6, 9} and Cs is additionally important for the management of risk after nuclear accidents.¹⁷⁻¹⁹ It is thus essential to consider these elements during the development of risk management strategies for (legacy) nuclear wastes, potential contamination and/or accidents.⁹ The mobility of Sr and Cs in soils and groundwater is controlled by surface reactions.^{17, 20} Sr complexes strongly with metal oxides (e.g. TiO₂, FeOOH, Fe₃O₄)²¹⁻²⁵ through surface complexation reactions, and with clay minerals (e.g., talc,¹⁷ illite, illite-smectite mixed layered phases,²⁵⁻²⁷ bentonite,²⁸ and kaolinite^{24, 29}) through both surface complexation and cation exchange reactions.^{17, 28, 30} Cs interacts strongly with clay minerals through cation exchange reactions^{17, 26, 31, 32} and through surface complexation on the basal surface of clay minerals.³³⁻³⁶ Furthermore, at low/trace concentrations, Cs can be irreversibly immobilized through diffusion into the interlayers of 2:1 clay minerals such as illite.³⁷ Such (surface) reactions can be heavily impacted by pH within the soils and groundwater,^{6, 16, 17, 25, 38} and by competing cations (such as Na and Ca).^{5, 6, 25, 27, 38} At elevated alkalinity (i.e. elevated pH and in a CO₂ rich atmosphere) Sr can be immobilized through the formation of strontianite (SrCO₃).^{24, 39, 40}

The components of colloidal silica gel, when injected into contaminated soils, will perturb the Sr and Cs geochemistry and the respective surface reactions. Silica nanoparticles within colloidal silica gel exhibit a large internal specific surface area, with an amorphous silica-like structure (potentially) available for Sr and Cs surface complexation.^{24, 39, 41} The porewater in gelled colloidal silica also has an elevated pH, potentially enhancing retention of Sr and Cs through increasing surface complexation to (clay) minerals and the silica nanoparticles (20, 21, 36-38).^{24, 25, 38, 39, 41} However, a high ionic strength due to a saline accelerant used to induce gelling^{5, 42} could cause (increased) competition between cations in the accelerant with contaminants for surface complexation processes⁴¹ inducing the release of Sr and Cs from mineral components into the colloidal silica porewater. This could lead to diffusion of contaminants through the gelled materials⁴² and subsequent release of radionuclides into the groundwater. Thus, a comprehensive understanding of these competing impacts on the geochemistry, fate, mobility and speciation of contaminants, such as Sr and Cs, is required to underpin the use of nanoparticulate colloidal silica materials for contaminant control.¹⁴⁻¹⁶

Here we investigated the competing impacts of colloidal silica gel on radionuclide mobility in clayey soil and waste materials. We performed a comprehensive set of experiments and complementary state-of-the-art analyses on the gelling of colloidal silica and the impacts on Sr and Cs geochemistry. First, Sr and Cs were adsorbed onto soil and waste materials (Table S1). Next, these contaminated solids were embedded in colloidal silica, gelled with either 1.4 M NaCl [Na-CS] or 0.175 M CaCl₂ [Ca-CS] as the accelerant. Subsequent leaching experiments were performed, including complementary XAS analyses, to determine the impacts of colloidal silica gel on the mobility and speciation of Sr and Cs.

Materials and methods

The minerals and solid materials used to create the solid mixtures (described in Table S1) were purchased from Sigma Aldrich except for the illite-smectite mixed layer (70/30 ordered), which was purchased from the Clay Mineral Society (special source clay: ISCz-1). These minerals and solids were mixed to simulate clayey soil and degraded waste compositions (Table S1). All chemicals used in the experimental methods were analytical grade reagents obtained from Sigma Aldrich, except for the Sr-85 and Cs-137 stock solutions which were obtained from Eckert-Ziegler, and the colloidal silica gel (MP 325), which was obtained from BASF. The colloidal silica nanoparticles, and the gelling of the colloidal silica with 1.4 M NaCl and with 0.175 M CaCl₂ in the accelerant were imaged using a Jeol 2100F transmission electron microscope (TEM) operating at 200 kV. Full details on the methods and the justification of the treatment of the data are described in the Electronic Supplementary Information.

Leaching Experiments

In order to produce contaminated solids, adsorption experiments were performed with 10 g/l of simulated clayey soil, simulated waste, or a mixture thereof (Table S1). These adsorption experiments were performed in a 10 mM NaCl solution at pH 7 either at trace (environmentally relevant) concentrations of Sr-85 and Cs-137 radiotracers (20 Bq/ml Sr-85 and Cs-137) or at elevated concentrations (to enable comparison with XAS analyses) of stable Sr and Cs (25 ppm Sr and Cs). After equilibrating these adsorption experiments for 48 hours, the pH was analysed, aqueous samples were taken for subsequent analyses and the contaminated solid samples were separated from the supernatant (Table S2). These solid samples were mixed with 5 ml colloidal silica and 1 ml of an accelerant consisting of either 1.4 M NaCl [Na-CS] or 0.175 M CaCl₂ [Ca-CS] to induce gelling of the colloidal silica. These samples cured for 7 days, after which leaching was induced by adding 20 ml of 10 mM NaCl as leaching solution/supernatant to the experiment. To mimic the respective interaction with flowing groundwater around a potential colloidal silica based barrier, a fixed volume of the supernatant was replaced for an equal volume of uncontaminated 10 mM NaCl over a four week [4wk] or a six month [6mth] period. While replacing the supernatant, the pH was determined and subsequently the composition of the

replaced supernatant was analysed. A set of parallel desorption experiments (at pH 6.5-7) on similar contaminated samples, which had not been embedded in colloidal silica gel, were performed over a two-week period. The experimental procedures of the leaching and parallel equilibrium desorption experiments are summarized in Table S3.

Aqueous analyses. The samples from the experiments at trace concentrations of Sr-85 and Cs-137 (20 Bq/ml) were acidified (with 0.1 ml concentrated HCl) prior to γ -spectroscopy to analyse for Sr-85 and Cs-137 (ORTEC P-type high purity germanium detector coupled to ORTEC DSPEC Pro digital spectrometers) and subsequent ICP-AES analyses for Ca and Na (Varian Vista AES). The activity concentrations of Sr-85 and Cs-137 were subsequently decay-corrected to correspond to the start of the adsorption experiments; all reported activity concentrations correspond to the total activity at the start of the adsorption experiments. The samples from the experiments at elevated concentrations of Sr and Cs (25 ppm) were filtered through 0.2 μm PVDF syringe filters prior to cation chromatography to analyse for Sr, Cs, Ca and Na (Metrohm 850 Professional IC AnCat, using a C6 cation exchange column and an eluent containing 4.5 mM HNO_3 and 1.5 mM dipicolinic acid).

X-ray absorption spectroscopy

X-ray absorption spectroscopy (XAS), is a powerful tool to determine the speciation of contaminants, including the respective mobility and bioavailability, and the impacts of environmental engineering strategies on the speciation of contaminants.^{16, 17, 20, 43} To produce samples for XAS analyses, complementary adsorption and leaching experiments were performed. Adsorption experiments were performed on soil samples at 25 ppm Cs and on soil/waste samples at 25 ppm Sr as described above. 0.4 g of the resulting contaminated samples (Table S2) were mixed with 0.333 ml of colloidal silica and 0.067 ml of either 1.4 M NaCl [Na-CS] or 0.175 M CaCl_2 [Ca-CS] as the accelerant within a 4 ml cryo-centrifuge tube, and cured for 7 days. Leaching of Sr or Cs was induced by submerging these 4 ml cryo-centrifuge tubes into 40 ml of 10 mM NaCl as the supernatant for 20 days. The pH was analysed and 2.5 ml of the supernatant was sampled 5 times over the 20 day duration and analysed as described above. After 20 days the 4 ml cryo-centrifuge tubes were collected, sealed and stored prior to XAS analyses.

X-ray absorption spectroscopy on samples and suitable standards (Table S4) was performed at the general purpose XAS beamline (B18) at Diamond Light Source⁴⁴ on the Cs K-edge (35,985 eV) using a Si(311) monochromator and the Sr K-edge (16,105 eV) using a Si(111) monochromator. The energy of the X-rays was calibrated using an yttrium foil (for the Sr K-edge) and an antimony foil (for the Cs K-edge). The samples were analysed for their spectra in fluorescence mode using a 36-element Ge detector, and the standards were analysed in transmission mode. The spectra were processed and analysed using the Demeter software package.⁴⁵ Athena was used for data reduction and background subtraction. Artemis was used to fit the Fourier Transform (in R-space) of the EXAFS spectra. FEFF6⁴⁶ was used to calculate the (initial) Sr and Cs scattering

paths using models / crystallographic information files for Sr and Cs, developed using illite crystallographic information.⁴⁷

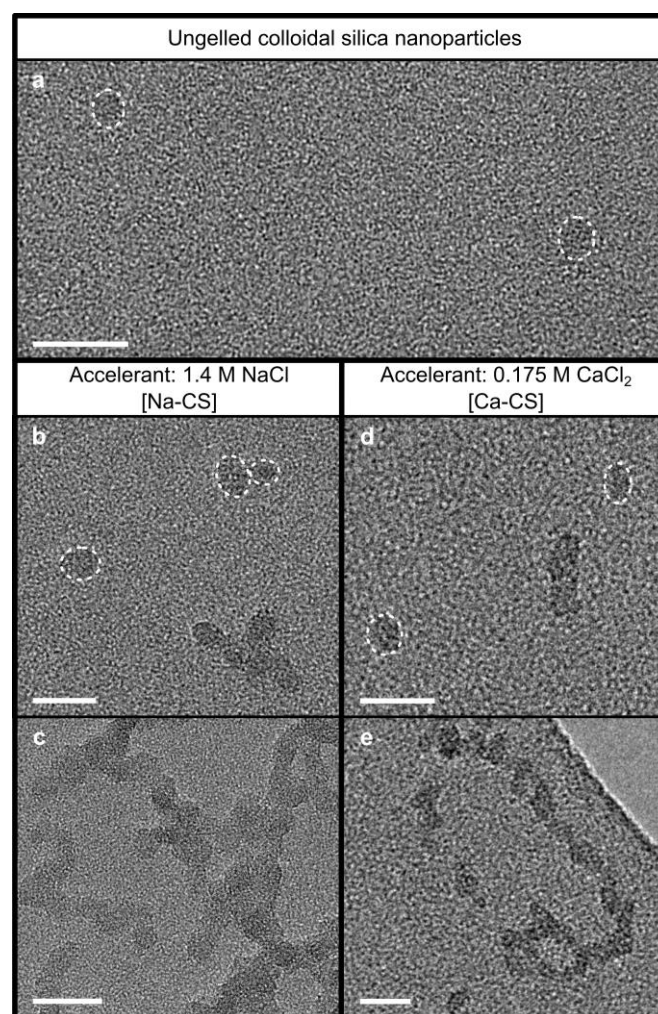


Fig. 1. TEM images from the colloidal silica gel used during the experiments, showing single 7.5 nm SiO_2 nanoparticles (a) which subsequently form clusters of nanoparticles after mixing the colloidal silica with an accelerant: (b) 1.4 M NaCl or (d) 0.175 M CaCl_2 , ending in gelled colloidal silica consisting of chains of colloidal silica (c and e). The scale bar in all TEM images represents 20 nm, and the dashed white circles were used to emphasize the presence of SiO_2 nanoparticles.

Results and discussion

Colloidal silica gelling and the properties of contaminated solid – colloidal silica gel systems

In this study we utilized a commercially available colloidal silica (MasterRoc MP 325)⁴⁸ which consists of a pH 10, 0.14 M Na^+ (from Na_2O) solution with 15 weight% dispersed silica nanoparticles (diameter: ~ 7.5 nm.; Fig. 1a). When mixing the colloidal silica with a saline solution (1.4 M NaCl or 0.175 M CaCl_2) as the accelerant, at a colloidal silica:accelerant ratio of 5:1 gelling is induced.^{12, 13} Cations within the saline accelerant cause a reduction in the negative ζ -potential of the silica nanoparticles⁴⁹⁻⁵³ through surface complexation with deprotonated silanol sites⁵² and a decrease in the thickness of the (electric) diffuse layer associated with negatively charged

silica surfaces.⁵⁰⁻⁵² This enables closer approach of the silica nanoparticles^{12, 13} and subsequent cluster formation (Fig. 1b and d). Diffusion limited cluster aggregation^{49, 51} then results in the formation of a fractal-like network of colloidal silica chains (Fig. 1c and e).⁴⁹ Concurrent to the cluster formation and aggregation processes, silica growth occurs around the contacts between silica nanoparticles (the formation of “necks”) (Fig. 1c and e) in order to reduce the interface curvature and thus minimize the surface free energy, e.g. through a monomer addition mechanism.^{54, 55} This gelling process results in the formation of a very low permeability silica hydrogel with an internal specific surface area of ~ 80 m²/ml and ~ 93 % (by volume) of interconnected nanopores saturated with saline water. The induction time to the gelling process can be controlled by varying the pH or the concentration and type of accelerant, such as 1.4 M NaCl (Fig. 1b and c) or 0.175 M CaCl₂ (Fig. 1d and e).¹² Once injected into a soil, gelling of the colloidal silica results in a very low permeability system that inhibits advective flow, which could make such a binary soil – colloidal silica gel system ideal for hydraulic barriers.

To determine the impacts of such binary soil – colloidal silica gel systems on radionuclide speciation and mobility (both for pre-existing radionuclides within a potential barrier and for radionuclides leached from wastes after barrier formation), we first produced contaminated samples with solid compositions representative of clayey soils at nuclear legacy sites⁹ and waste materials likely present at such sites. These contaminated samples were produced by performing a set of adsorption experiments on model soil minerals and waste components (Table S1) at (environmentally relevant) trace concentrations (using radiotracers: Sr-85 and Cs-137) and at elevated concentrations (to enable comparison with subsequent XAS analyses). The results of these initial adsorption experiments (Table S2) show distribution coefficients (K_D) at values comparable to previous experiments on single clay mineral phases and soils, and from surface complexation modelling.^{18, 21, 26, 27, 31, 32, 38} Comparing the K_D values of the contaminated soil with previous studies, indicates that for the soil and soil/waste mixtures the mobility of Sr and Cs is dominated by their interaction with clay minerals, e.g. through surface complexation on the basal surface^{34, 35} and potentially incorporation into the interlayer.^{25, 28, 37} In the absence of clay minerals, the K_D values are lower and likely governed by the interaction of Cs and Sr with metal oxide phases (i.e. magnetite, Fe₃O₄).²¹ To create the binary contaminated solid – colloidal silica gel samples for subsequent leaching experiments, we then embedded these contaminated solids (Table S2) within colloidal silica gel and induced gelling with either 1.4 M NaCl [Na-CS] (Fig. 1b and c) or 0.175 M CaCl₂ [Ca-CS] (Fig. 1d and e) as the accelerant.

Leaching experiments on contaminated solid – colloidal silica systems

Leaching experiments on the binary systems containing colloidal silica gel and contaminated solids were performed with 10 mM NaCl. To mimic the interaction of the solids with uncontaminated mobile groundwater, the supernatant was

repeatedly replaced with an equal volume of uncontaminated 10 mM NaCl. During the replacement of the supernatant, the solutions were analysed for the pH and subsequently for their cation composition. The leaching experiments had a total duration of four weeks [4wk] or six months [6mth] (trace Sr and Cs contamination only, to determine the influences of rate vs. equilibrium behaviour). To evaluate the impacts of colloidal silica on Sr and Cs geochemistry, parallel equilibrium desorption experiments (without colloidal silica) were performed so that impacts of the colloidal silica gel on the mobility of Sr and Cs could be determined. To inform on these impacts we used their aqueous concentrations in the supernatant to calculate the apparent distribution coefficients and compare these to the K_D values from the parallel equilibrium desorption experiments. Full details of these experiments are given in the Methods and Materials and summarized in Table S3.

The results from the leaching and equilibrium desorption experiments are summarized in Fig. 2 and Table S2. In brief, the apparent Sr and Cs K_D values vary between those experiments conducted at trace concentrations and those conducted at elevated Sr and Cs concentrations (Fig. 2), as well as between the 4wk and the 6mth experiments. In the presence of colloidal silica, the (final) apparent K_D values were up to 2 orders of magnitude higher for Sr and up to 1 order of magnitude higher for Cs compared to the K_D values obtained from the parallel equilibrium desorption experiments (without colloidal silica gel). Moreover, in all cases, the (final) apparent K_D values were in excess of those obtained from the parallel equilibrium desorption experiments. This suggests that the colloidal silica, including the impacts of the porewater geochemistry (i.e. pH and competing cations from the accelerant) improved the capacity of the contaminated solid – colloidal silica gel systems to retain and immobilize Sr and Cs.

The pH remained relatively stable during the leaching experiments at elevated (mg/g) Sr and Cs concentrations (Fig. 2a and e). Only a small initial pH increase, from 9.5 up to ~ 10 was observed (Fig. 2a and e) during the initial stage of equilibration between the supernatant and the porewater geochemistry. After this, the pH gradually decreased to 9.5, due to the continued removal of OH⁻ while replacing the supernatant. The relatively stable pH during these experiments was caused by a high buffer capacity of the colloidal silica gel and a limited exchange with atmospheric CO₂. Conversely, because the leaching experiments at trace Sr and Cs contamination were continuously exposed to atmospheric CO₂ (to more closely represent environmental conditions), the continuous ingress of acidic CO₂ caused the pH in these experiments to decrease to ~ 8 (Fig. 2a and e). Finally, the differences between the 4wk and 6mth leaching experiments at trace Sr and Cs contamination allowed more CO₂ to diffuse into the supernatant and the porewater between each point the supernatant was replaced, thus during the 6mth leaching experiment the initial increase in pH is absent.

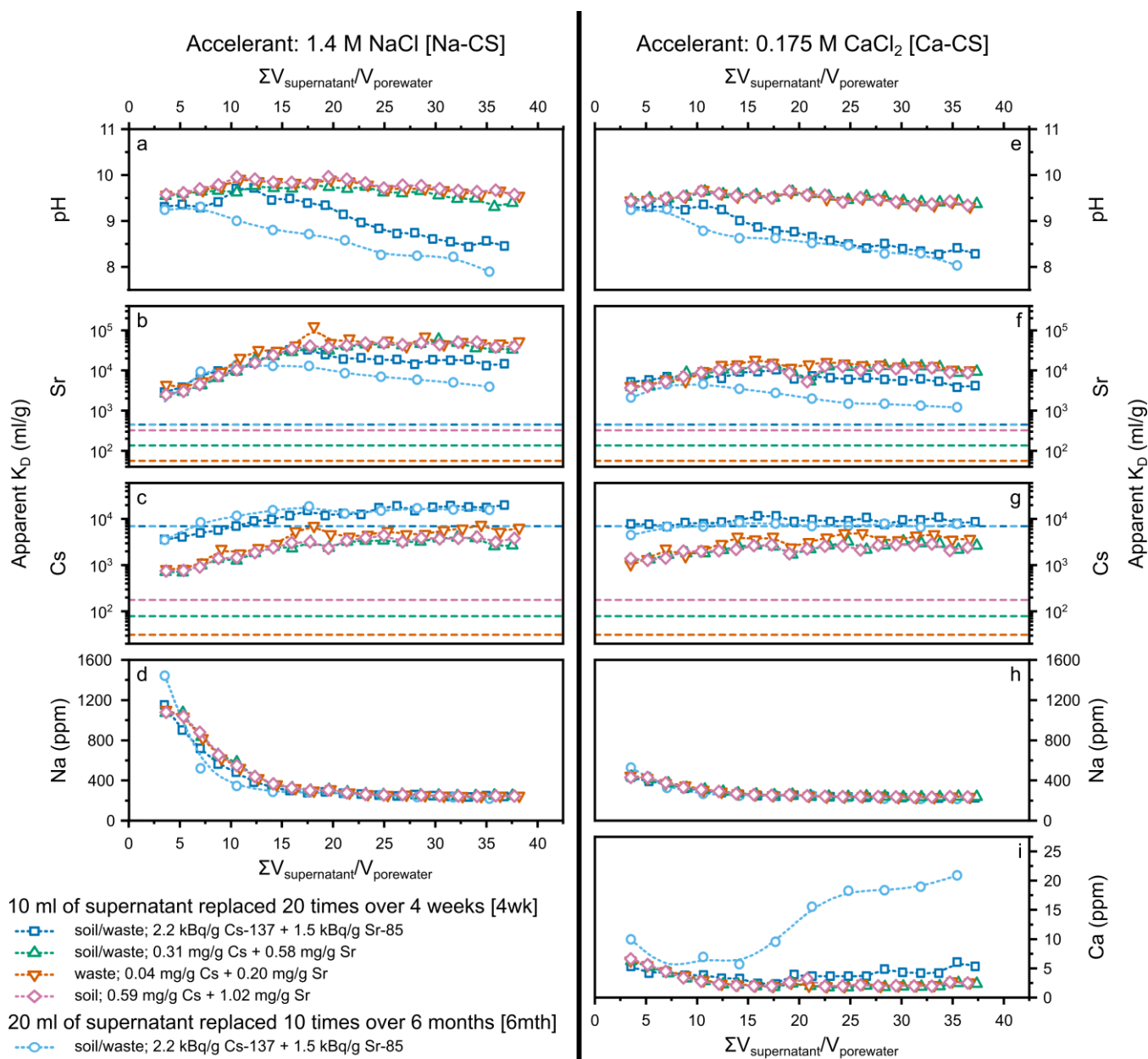


Fig. 2. Summary of the aqueous analyses on all leaching experiments performed over 4 weeks [4wk] and 6 months [6mth] using colloidal silica gelled with 1.4 M NaCl [Na-CS] (a-d) and with 0.175 M CaCl₂ [Ca-CS] (e-i). The pH (a, e), apparent K_D values for Sr (b, f) and Cs (c, g), the Na concentration in the supernatant (d, h) and the Ca concentration in the supernatant (i) are plotted against the cumulative volume of the leaching solution/supernatant divided by the pore volume within the gelled colloidal silica ($\Sigma V_{\text{supernatant}}/V_{\text{porewater}}$) as a qualitative measure of the amount of uncontaminated groundwater interaction with a potential colloidal silica based barrier, and to enable direct comparison between the different sampling/supernatant replacement regimes at trace (kBq/g) contamination. The legend describes the sampling regime [4wk vs. 6mth] and the composition of the original contaminated solid on which the leaching experiments were performed. The title above the graphs describe the accelerant used to gel the colloidal silica [Na-CS vs. Ca-CS]. The horizontal dashed lines in b, c, f and g represent the parallel desorption K_D values in which colours refer to the composition of the original contaminated solid used in the desorption experiment (see legend).

During all leaching experiments, Na from the accelerant (Na-CS) and/or the colloidal silica (Na-CS and Ca-CS) is released into the supernatant. Over time, the (measured) Na concentration in the supernatant decreased to approach that of the uncontaminated supernatant (10 mM/230 ppm Na; Fig. 2d and h). For all experimental conditions used (trace vs. elevated Sr and Cs contamination; Na-CS vs. Ca-CS; 4wk vs. 6mth), very similar results were observed. This suggests that neither the time

interval between supernatant replacement points, nor the variations in the pH affected the release of Na from the colloidal silica porewater. Rather, this suggests that the release of Na from the colloidal silica was governed by equilibrium conditions throughout all leaching experiments. In contrast, the Ca concentrations during the Ca-CS leaching experiments do show significant differences depending on the level of Sr and Cs contamination and between the 4wk and 6mth leaching

experiments (Fig. 2i). Briefly, there is an increase in the Ca concentration during the leaching experiments at trace Sr and Cs contamination (exposed to atmospheric CO₂, Fig. 2i). Furthermore, of these two leaching experiments, the 6mth leaching experiment showed the largest increase in the Ca concentration (Fig. 2i). These two observations suggest that both pH variations due to CO₂ ingress and rate constraints influence the release of Ca from the colloidal silica porewater.

The impacts of colloidal silica gel on the apparent K_D values at elevated Sr and Cs contamination. For the solid – colloidal silica gel systems at elevated levels of Sr and Cs contamination, the apparent K_D values during the Na-CS leaching experiments increased from $3.2 \pm 0.7 \cdot 10^3$ ml/g and stabilized at $4.6 \pm 0.8 \cdot 10^4$ ml/g for Sr, and from $7.7 \pm 0.5 \cdot 10^2$ ml/g and stabilized at $4 \pm 1 \cdot 10^3$ ml/g for Cs (Fig. 2b and c). During the Ca-CS leaching experiments, a similar trend was observed: the apparent K_D values increased from $4.0 \pm 0.2 \cdot 10^3$ ml/g and stabilized at $1.2 \pm 0.2 \cdot 10^4$ ml/g for Sr, and from $1.3 \pm 0.1 \cdot 10^3$ ml/g and stabilized at $3.1 \pm 0.9 \cdot 10^3$ ml/g for Cs (Fig. 2f and g).

In all cases, the apparent Sr K_D values were higher compared to the parallel equilibrium desorption K_D values (dashed horizontal lines in Fig. 2b,c,f,g and Table S2). The evolution of the apparent Sr and Cs K_D values from these leaching experiments did not vary significantly with the composition of the solid materials (including the presence or absence of clay minerals, Table S1). Conversely, the composition of the solid materials did impact on the initial level of contamination (0.20–1.02 mg/g Sr and 0.04–0.59 mg/g Cs; Table S2) and their equilibrium desorption K_D values (dashed horizontal lines Fig. 2b,c,f,g, Table S2). These observations show that the initial solid composition had a limited role in the leaching (and mobility) of Sr and Cs from the contaminated solid – colloidal silica gel system. This indicates that the silica nanoparticles provided surface complexation sites for Sr^{24,39} and Cs.⁴¹ This is likely aided by the elevated pH throughout these leaching experiments (Fig. 2a and e), improving the capacity of the contaminated solids to immobilize Sr and Cs.

The decrease in the Na concentrations in the supernatant during the Na-CS and the Ca-CS leaching experiments coincided with the increase in the apparent Sr and Cs K_D values (Fig. 2b-d,f-i). This difference is emphasized in Fig. 3a and b when plotting the apparent Cs K_D values against the Na concentration in the supernatant, including the respective inverse power regressions. This suggests that Na competed with Sr and Cs for adsorption sites, and a decrease in the Na content of the solid – colloidal silica gel system provided an increase in Sr and Cs adsorption sites and respective apparent K_D values. This confirms that competition of Sr and Cs with cations in the accelerant impact on their speciation and mobility, as suggested by Hakem et al.⁵ from batch adsorption experiments.

During the initial stages of the Na-CS leaching experiments, the apparent Cs K_D values were significantly lower compared to the Ca-CS experiment (Fig. 2c and g). This difference disappeared once the Na concentration in the supernatant (released from the accelerant and from the colloidal silica) approached ~230 ppm (10 mM) in both sets of experiments (Fig. 2c and g). The inverse power regressions in Fig. 3a emphasize that Na

competed for Cs adsorption to the solid materials within the samples. Additionally, the minimal differences in the regressions between the Na-CS and Ca-CS leaching experiments (Fig. 3a) suggest that Ca had a minor impact on the mobility of Cs within gelled colloidal silica. This shows that Ca did not significantly compete with Cs for adsorption sites in the contaminated solid – colloidal silica gel systems.

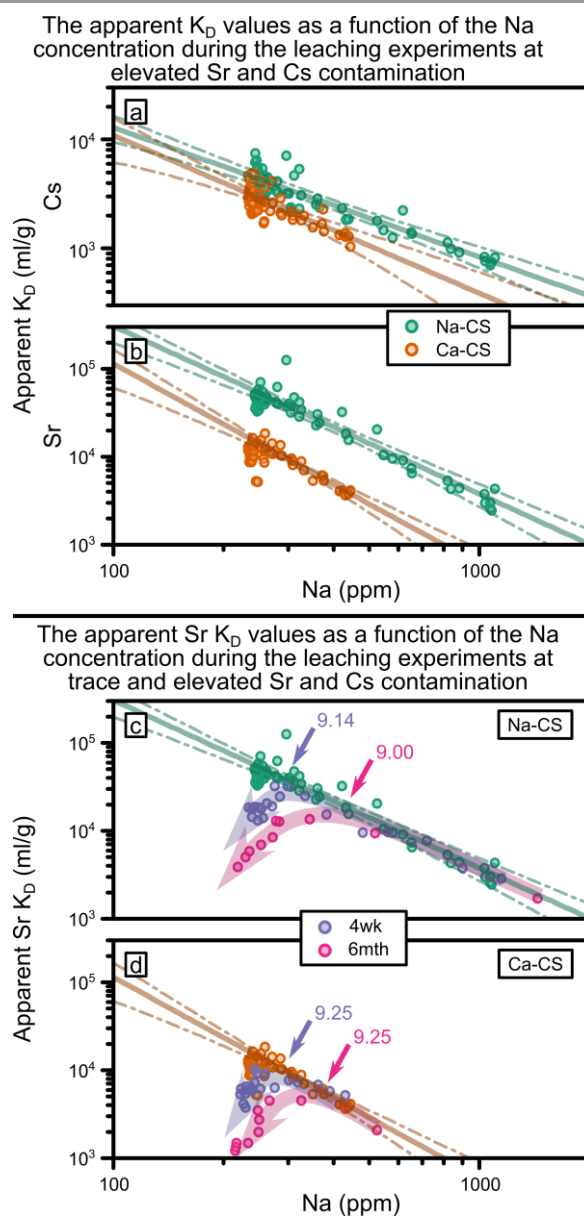


Fig. 3. The apparent K_D values from the leaching experiments (Fig. 2b,c,f,g) as a function of the Na concentration as measured in the supernatant (Fig. 2d and h) plotted on a log-log scale. Panels a and b: The apparent K_D values for Cs (a) and Sr (b) from all the leaching experiments at elevated Sr and Cs contamination for the Na-CS (green) and the Ca-CS (orange) leaching experiments, including power regressions (solid opaque lines) and their respective 99% confidence intervals (dash-dotted opaque lines). Panels c and d: The apparent Sr K_D values from the leaching experiments at trace Sr and Cs contamination during the 4wk and 6mth experiments are plotted for Na-CS (c) and Ca-CS (d), including the apparent Sr K_D values from the leaching experiments at elevated Sr and Cs contamination (colours are identical to b), the opaque curved arrows show the deviation of the apparent Sr K_D values from the regression (b) and are intended as a visual guide only, the arrows and numbers represent the pH values of the supernatant when the apparent Sr K_D values deviated from the regression.

During the initial stages of the Na-CS and the Ca-CS leaching experiments the apparent Sr K_D values are similar (Fig. 2b and f). However, the apparent Sr K_D values stabilized at higher values during the Na-CS experiments as compared to the Ca-CS experiments (Fig. 2b and f). Furthermore, when plotting the apparent Sr K_D values against the Na concentration (Fig. 3b) an inverse power relationship similar to Cs can be observed. This emphasizes that Na competed with Sr for adsorption onto the solid materials (Fig. 3b). Conversely, a large difference is observed in the inverse power regression between the Na-CS and Ca-CS leaching experiments (Fig. 3b), suggesting that Ca competed strongly with Sr for adsorption onto the solid phases throughout the leaching experiments. This competition resulted in significantly lower apparent Sr K_D values when Ca was used as the accelerant to induce gelling of the colloidal silica in the preparation of the binary contaminated solid – colloidal silica systems.

The impacts of colloidal silica gel on the apparent K_D values at trace/environmental Sr and Cs contamination. The leaching experiments on the trace Sr and Cs contaminated solid – colloidal silica gel systems were performed with two different durations of 4 weeks (4wk) and 6 months (6mth), and corresponding different times between each supernatant replacement point (Fig. 2 b,c,f,g). The apparent Cs K_D values during these experiments did not differ between the 4wk and 6mth experiments (Fig. 2c and g). This suggests that at trace levels of contamination, Cs leaching and mobility are governed by (surface) thermodynamic rather than rate/kinetic constraints.

During the Ca-CS leaching experiments, the apparent Cs K_D values were constant throughout the leaching experiments ($9 \pm 1 \cdot 10^3$ ml/g; Fig. 2g) at approximately the same value as the K_D value from the parallel equilibrium desorption experiment ($7 \pm 2 \cdot 10^3$ ml/g; Fig. 2g and Table S2). This suggests that the presence of Ca in the Ca-CS leaching experiments did not compete with Cs for adsorption or ion exchange sites. Interestingly, at trace concentrations in the batch adsorption experiments of Hakem et al.,⁵ in the absence of illite or illite-smectite phases, a decrease in the Cs K_D was observed for a soil – colloidal silica gel system with Ca in the accelerant. This implies that in the presence of illite or illite-smectite phases (Table S1) the apparent Cs K_D value was governed by the illite-smectite phase, likely through incorporation into their interlayers (inaccessible for Ca).³⁷

During the Na-CS leaching experiments, the apparent Cs K_D value was initially lower ($3.6 \pm 0.1 \cdot 10^3$ ml/g; Fig. 2c) than the K_D value from the parallel equilibrium desorption experiment ($7 \pm 2 \cdot 10^3$ ml/g) but steadily increased to a higher value ($1.6 \pm 0.2 \cdot 10^4$ ml/g) (Fig. 2c and g). This steady increase was concurrent with a decrease of the Na concentration in the supernatant (Fig. 2d). When comparing this to the Ca-CS leaching experiments, these observations imply that initially, competition between Na and Cs decreased the apparent K_D values compared to the parallel desorption experiments. However, during the latter stages of the experiments, once the Na concentrations were similar between the Na-CS and the Ca-CS leaching experiments, the elevated apparent Cs K_D values in

the Na-CS system (Fig. 2c and g) suggest Cs was not being released from the illite-smectite interlayers. Recent studies have shown that due to the small ionic radius of Na compared to Cs,⁵⁶ interaction of Na with the frayed edge sites on 2:1 clay minerals (like illite) can induce a collapse of the frayed edge sites,⁵⁷ blocking the release of Cs from interlayer sites.⁵⁸ These observations suggest that once the Na concentration decreased sufficiently, the collapsed frayed edges prevented leaching of the remaining Cs from the interlayer of the illite-smectite phase³⁷ resulting in the observed increase in the apparent Cs K_D values (Fig. 2c). This hypothesis is further supported by a direct comparison of the Cs K_D values from the parallel equilibrium desorption experiments using deionised water (18.2 M Ω , DI), and 10 mM NaCl as the supernatant (in Table S2); in DI, where Na is not present, the K_D value was significantly lower.

At trace Sr and Cs contamination, the apparent Sr K_D values initially appear to mimic the trends observed during the experiments at elevated Sr and Cs contamination (Fig. 2b and f). This suggests that, initially, the silica nanoparticles control the leaching of Sr. However, once the pH in the supernatant drops below 9.0-9.3 due to the ingress of atmospheric CO₂, the apparent Sr K_D values deviated from the experiments at elevated concentrations (Fig. 2a,b,e,f, Fig. 3c and d). During the Na-CS leaching experiments, the apparent Sr K_D continues to decrease to values of $1 \cdot 10^4$ ml/g or $4 \cdot 10^3$ ml/g in the 4wk or 6mth experiments, respectively (Fig. 2b). During the Ca-CS leaching experiments, the apparent K_D values decreased to values of $4 \cdot 10^3$ ml/g or $1 \cdot 10^3$ ml/g in the 4wk or 6mth experiments, respectively (Fig. 2f). These trends are further illustrated in Fig. 3c and d by the deviation from the inverse power regression observed in the apparent Sr K_D values during the leaching experiments at elevated Sr and Cs contamination (as emphasized by the opaque arrows). The pH values (pH 9.0-9.3) below which the apparent Sr K_D values deviate from the power regression (Fig. 3c and d) correspond with the adsorption edges for Sr adsorption to amorphous silica.³⁹ Hence, for Sr at trace level contamination, the observed decrease in the apparent K_D values was likely a result of pH induced desorption of Sr from the silica nanoparticle surfaces.

Finally, for the Na-CS and the Ca-CS leaching experiments, the final pH values in, both, the 4wk and 6mth leaching experiments were pH 8-8.5 compared to 9.5-10 during the leaching experiments at elevated Sr and Cs contamination (Fig. 2a and e). However, the difference between the final apparent Sr K_D values was larger between the 4wk and 6mth experiments compared to the leaching experiments at elevated Sr and Cs contamination. The final apparent Sr K_D values were significantly lower for the 6mth leaching experiments than the 4wk leaching experiments (Fig. 2b and f and Fig. 3c and d). This indicates that the duration between each point when the supernatant was replaced (and the resulting equilibration time) impacted on the quantity of Sr leached from the soil/waste samples, and that rate constraints influenced the release of Sr. Possible rate-limiting reactions are desorption of Sr from the silica nanoparticles and the diffusion of Sr through the colloidal silica porewater. Nevertheless, even in the 6mth experiments, the apparent Sr K_D values continuously exceeded the K_D values

from the parallel equilibrium desorption experiments (Fig. 2b and f, Table S2). This suggests that even at these lower pH values, silica nanoparticles provided abundant sites for Sr adsorption.

Sr and Cs speciation through X-ray absorption spectroscopy (XAS)

To further develop (and validate) our conceptual model on the impacts of colloidal silica on the geochemistry of Sr and Cs, we performed a complementary set of leaching experiments to produce samples suitable for Sr and Cs K-edge XAS. To optimize the respective samples for Sr and Cs XAS analyses, these experiments involved separately adsorbing Sr or Cs to produce the contaminated samples (to prevent potential competition between Sr and Cs for adsorption sites, Table S2). These contaminated solid samples were embedded in a proportionally smaller amount of colloidal silica (minimizing the dilution of the Sr or Cs concentration). Aqueous samples to analyse for the apparent K_D values were obtained without replacing the supernatant to prevent excessive cumulative Sr and Cs leaching. Fig. S1 summarizes the results from these leaching experiments (apparent K_D values and Na and Ca concentrations). Briefly, due to the smaller amount of colloidal silica gel and without supernatant replacement, the absolute apparent Sr and Cs K_D values were different compared to the previous Sr and Cs leaching experiments (Fig. 2). However, the initial apparent K_D values are of the same order of magnitude and the apparent K_D values show the same variability between Na-CS and Ca-CS. Hence, the same processes control the leaching of Sr and Cs in these experiments (more details are described in the ESI).

The Sr K-edge XAS data are summarized in Fig. 4. The X-ray absorption near edge structure (XANES) show very similar spectra for all the soil/waste samples (#2-6, Fig. 4a), the

colloidal silica gelled with 0.2 M SrCl_2 (#1, Fig. 4a) and the aqueous Sr^{2+} standard (10,000 ppm Sr^{2+} as SrCl_2 ; #7, Fig. 4a). The XANES for strontianite (SrCO_3) is distinct from the other XANES as it exhibits a broader minimum in the XANES between 16,130 and 16,140 eV (#8, Fig. 4a). This shows that no strontianite formed during these leaching experiments.

For all Sr K-edge EXAFS spectra the closest scattering path could be fit with 9 oxygen backscatterers at 2.59-2.61 Å, corresponding to published values for aqueous Sr^{2+} and Sr surface complexes of 2.57-2.63 Å.^{24, 25, 39, 59, 60} The EXAFS spectrum of the aqueous Sr^{2+} standard could be fitted with 9 oxygen backscatterers at 2.590 Å (Table 1, Fig. 4b and c), highlighting the fully hydrated nature of aqueous Sr^{2+} . The spectrum to the colloidal silica gelled with 0.2 M SrCl_2 could be fitted with 9 oxygen backscatterers at 2.609 Å, only (Table 1, Fig. 4b and c). This suggests the presence of fully hydrated Sr^{2+} ions complexed with silica nanoparticles, through the formation of outer-sphere surface complexes. This is consistent with previous EXAFS analyses on Sr adsorption to amorphous silica.^{16, 17, 24, 39} Due to the chemical similarities between Sr and Ca, the formation of such outer-sphere surface complexes with the silica nanoparticles likely also occurred during the gelling of Ca-CS. We thus propose that the formation of such outer-sphere surface complexes decreases the ζ -potential of silica nanoparticles when a divalent cation is used in the accelerant.⁵⁰ This subsequently decreases the effective negative charge of the silica nanoparticles, and hence induces cluster formation and subsequent cluster aggregation (as shown for Ca in Fig. 1d and e) during the gelling process of colloidal silica.^{49, 51}

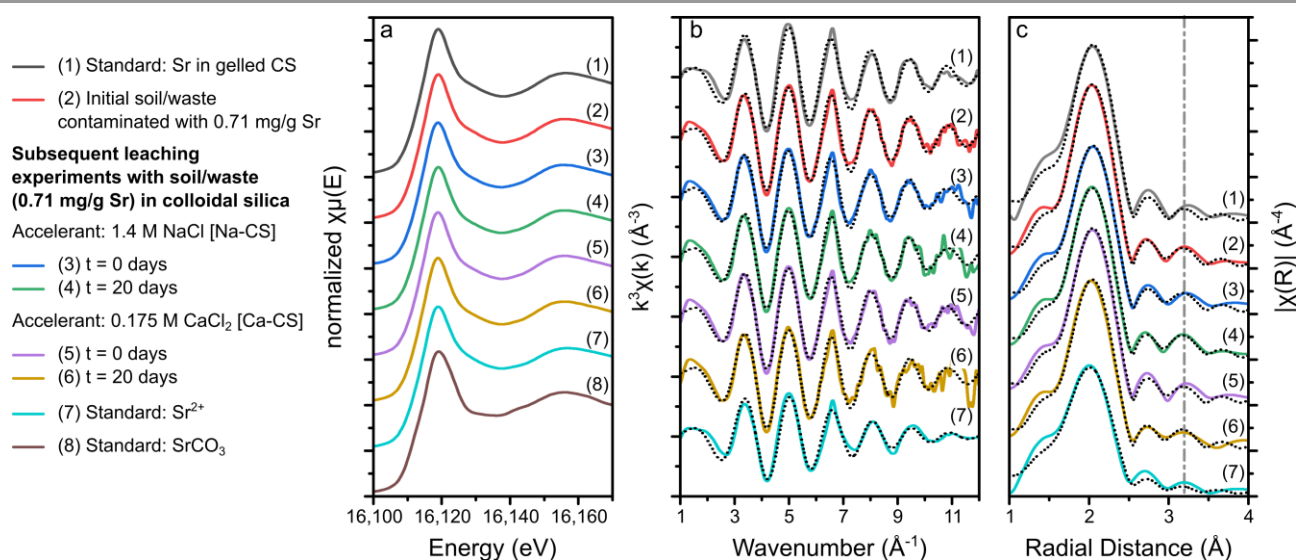


Fig. 4. Summary of the results from the Sr K-edge XAS analyses. The solid coloured lines represent the XANES (a), EXAFS in k-space (b) and the amplitude of the Fourier Transform of the EXAFS in R-space (non-phase corrected) (c) of the samples and standards, the black dotted lines represent the fits to the EXAFS spectra and the dash-dotted line highlights the position of the Sr-Si/Al scattering path (Table 1).

The Sr K-edge EXAFS for all samples (initial soil/waste sample and the respective samples in the Na-CS and Ca-CS leaching experiments before and after 20 days of leaching) could be fitted with 9 oxygen backscatterers at 2.602–2.610 Å and a single Si/Al backscatterer at 3.78–3.80 Å (Table 1, Fig. 4b and c). The absence of any Sr–C and Sr–Sr backscatterers confirms the observation from the XANES spectra (Fig. 4a) that no strontianite formed during the leaching experiments, and the presence of the Sr–Si/Al backscatterers at 3.78–3.79 Å indicate that Sr interacts with the solid materials through the formation of an inner-sphere surface complex with phyllosilicate minerals such as clay minerals, similar to the complexation of Sr with chlorite.²⁵ This appears to occur irrespective of competition with Na and/or Ca within the Na-CS or Ca-CS samples, or the subsequent leaching experiments. Therefore, throughout these leaching experiments, inner-sphere surface complexes with clay minerals dominated Sr speciation. It should, however, be noted that EXAFS only provides the average coordination environment and fitting EXAFS generally reveals the dominant coordination environment only.^{61–63} Interestingly, the fits to R-space for the Sr–Si/Al scattering path showed a small mismatch with the data for the samples from the Na-CS and the Ca-CS experiments at $t = 0$ days (vertical dash-dotted line; #3 and 5, Fig. 4c), including a decrease in the statistical confidence that the addition of a Sr–Si/Al backscatterer improved the fit (Table S5). Furthermore, the Sr–O radial distances in these $t = 0$ days samples (2.608–2.610 Å), appear to more closely match the Sr–O radial distance of the colloidal silica standard (2.609 Å) than aqueous Sr²⁺ (2.590 Å, Table 1). These two observations could suggest the presence of an additional Sr surface species, such as outer-sphere surface complexes to silica nanoparticles,^{24, 39} rather than Sr in the porewater. The observed small mismatch disappeared in the samples after 20 days of leaching concurrent to an increase in the statistical confidence that the addition of a Sr–Si/Al backscatterer improved the fit (Table S5), and the Sr–O radial distances (2.602–2.603 Å) more closely match the Sr–O radial distances of the initial soil/waste sample (2.603 Å, Table 1). This suggests that after 20 days the fraction of Sr adsorbed to colloidal silica nanoparticles decreased, caused by a decrease in the porewater pH below the adsorption edge of Sr adsorption to amorphous silica.^{24, 39} This pH dependent decrease in Sr outer-sphere complexation to the silica nanoparticles likely caused the observed decrease in the apparent K_D values during the leaching experiments (Fig. S1a). These results show that inner-sphere surface complexation with phyllosilicate minerals controls the mobility of Sr while the colloidal silica can provide additional surface complexation sites for Sr immobilization,

specifically at elevated pH values (i.e. above the Sr adsorption edge for amorphous silica^{24, 39}).

Table 1. Summary of the fits to the Sr and Cs K-edge EXAFS data; the amplitude correction factor was fixed to 1, C.N. represents the coordination number (fixed, the errors on the C.N. are estimated to be ~25%), ΔE_0 the energy shift, R the radial distance and σ^2 the Debye-Waller factor, the numbers in parentheses are the uncertainties as calculated by Artemis,⁴⁵ and the fit ranges and the goodness of fit parameters are described in Table S5.

Sample	ΔE_0 (eV)	Path	C.N.	R (Å)	σ^2 (Å ²)
Sr in gelled colloidal silica	-2.9(6)	Sr–O	9	2.609(6)	0.0086(4)
Soil/waste; 0.71 mg/g Sr	-3.4(3)	Sr–O	9	2.603(4)	0.0082(3)
		Sr–Si/Al	1	3.78(3)	0.011(4)
Soil/waste; 0.71 mg/g Sr; Na-CS; t = 0 days	-3.1(4)	Sr–O	9	2.610(5)	0.0093(3)
		Sr–Si/Al	1	3.80(3)	0.009(4)
Soil/waste; 0.71 mg/g Sr; Na-CS; t = 20 days	-3.5(3)	Sr–O	9	2.603(3)	0.0091(2)
		Sr–Si/Al	1	3.80(2)	0.007(2)
Soil/waste; 0.71 mg/g Sr; Ca-CS; t = 0 days	-3.1(5)	Sr–O	9	2.608(6)	0.0087(4)
		Sr–Si/Al	1	3.79(5)	0.012(7)
Soil/waste; 0.71 mg/g Sr; Ca-CS; t = 20 days	-3.3(4)	Sr–O	9	2.602(5)	0.0091(3)
		Sr–Si/Al	1	3.80(4)	0.010(5)
Sr²⁺	-3.9(8)	Sr–O	9	2.590(9)	0.0127(6)
SrCO₃[§]		Sr–O	9	2.56–2.73	-
		Sr–C	3	3.03–3.04	-
		Sr–Sr	4	4.09–4.12	-
		Sr–Sr	2	4.24	-
		Sr–Sr	4	4.89	-
Cs in gelled colloidal silica	8.0(8)	Cs–O	9	3.25(2)	0.025(1)
		Cs–Si	2	4.04(4)	0.023(7)
		Cs–Cs	1	4.26(2)	0.006(1) [#]
		Cs–Cs	1	4.56(2)	0.006(1) [#]
		Cs–Si/Al	5.5	4.13(4)	0.015(1) [~]
Soil; 0.84 mg/g Cs	1.4(30)	Cs–O	8	3.15(3)	0.019(1) [*]
		Cs–O	4	3.43(3)	0.019(1) [*]
Soil; 0.84 mg/g Cs; Na-CS; t = 0 days	3.1(39)	Cs–O	8	3.09(4)	0.019(1) [*]
		Cs–O	4	3.45(4)	0.019(1) [*]
		Cs–Si/Al	3.5	4.01(6)	0.015(1) [~]
Soil; 0.84 mg/g Cs; Na-CS; t = 20 days	0.7(49)	Cs–O	8	3.12(5)	0.019(1) [*]
		Cs–O	4	3.37(6)	0.019(1) [*]
		Cs–Si/Al	4	4.08(6)	0.015(1) [~]
Cs⁺	6.1(5)	Cs–O	5	3.10(1)	0.020(1)
		Cs–O	5	3.36(2)	0.027(2)

[§]The strontianite radial distances are based on its crystallographic information.^{64–66}

*The σ^2 from the Cs–Cs scattering paths for Cs in gelled colloidal silica were simultaneously fitted to the same value to reduce the number of independent variables.

[#]The σ^2 from the Cs–O scattering paths in all soil samples were simultaneously fitted to the same value.

[~]The σ^2 for the Cs–Si/Al scattering paths in all the soil samples were simultaneously fitted to the same value.

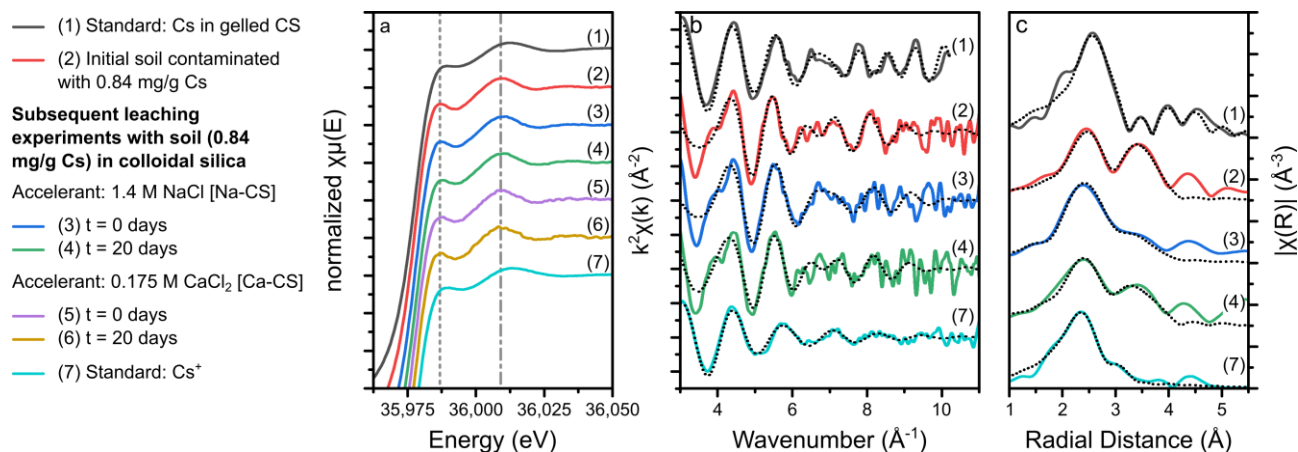


Fig. 5. Summary of the results from the Cs K-edge XAS analyses (a-c). The solid coloured lines represent the XANES (a), EXAFS in k-space (b) and the amplitude of the Fourier Transform of the EXAFS in R-space (non-phase corrected) (c) of the samples and standards and the black dotted lines represent the fits to the EXAFS spectra. The vertical dashed lines (a) highlight the white line and the position of the first scattering feature in the Cs K-edge XANES.

The Cs K-edge XAS data are summarized in Fig. 5. The XANES from all the soil samples (#2-6, Fig. 5a) exhibit a more pronounced white line (dashed line, Fig. 5a) and a first scattering feature shifted to lower energies (dash-dotted line, Fig. 5a) compared to the XANES from the aqueous Cs⁺ (10,000 ppm Cs⁺ as CsCl) and the colloidal silica standards (#1 and 7, Fig. 5). This indicates that the Cs speciation in the soil samples did not vary between and during the Na-CS and Ca-CS leaching experiments and was distinct from aqueous Cs⁺ and Cs within colloidal silica only. The Cs K-edge EXAFS spectrum from the aqueous standard could be fit with two Cs-O scattering paths at 3.10 and at 3.36 Å, with no additional scattering paths at larger radial distances (Table 1, Fig. 5b and c), highlighting the hydrated nature of aqueous Cs⁺. The EXAFS spectrum for Cs in colloidal silica could be fitted with a single Cs-O scattering path at 3.25 Å, two additional Si backscatterers at 4.04 Å, and two Cs backscatterers at 4.26 and at 4.56 Å (Table 1, Fig. 5b and c). The radial distance of the Cs-O scattering path appears intermediate between published Cs-O radial distances for aqueous and adsorbed Cs of 3.00-3.21 Å,^{37, 67, 68} and in hydrated CsOH solids of 3.34-3.45 Å.^{69, 70} This Cs-O radial distance in combination with the fitted Cs-Si and Cs-Cs scattering paths suggests that when 0.8 M CsCl is used as an accelerant, Cs interacts strongly with the colloidal silica nanoparticles through the formation of multinuclear surface species (e.g. surface clusters, potentially intermediate between a solid and adsorbed species). This appears to be consistent with reported complexation of several metals with silicate phases such as the complexation of Cr with amorphous silica,⁷¹ Co with kaolinite^{72, 73} and U and Eu with clinoptilite.⁷⁴ The formation of such surface clusters is thus the likely mechanism by which Cs impacted on the ζ-potential of silica nanoparticles, which induced cluster formation and subsequent cluster aggregation (as shown for Na in Fig. 1b and c) during the gelling process. Furthermore, as there is no significant difference in the mechanisms when varying between different alkali metals (e.g. Na and K) in the accelerant,^{49, 51} we postulate that the formation of such multinuclear surface

species could also induce gelling when NaCl is used as the accelerant.

The Cs K-edge EXAFS from the soil sample (#2, Fig. 5b and c) could be fitted with two Cs-O scattering paths at 3.15 Å and at 3.43 Å. Furthermore, 5.5 Si/Al backscatterers at 4.13 Å were required in the fit (Table 1). These radial distances and the respective coordination numbers are consistent with previous molecular dynamics studies for Cs adsorption onto the basal surface of illite,³⁴ and kaolinite³⁵ through inner-sphere surface complexes at the Si vacancy sites. This highlights that Cs speciation (and thus its respective mobility) within our (simulated clayey) soil samples was governed through the formation of inner-sphere surface complexes on the basal surface of clay minerals (i.e. illite-smectite and kaolinite).

Due to constraints on analysing the high energy of the Cs K-edge,³⁷ we were only able to analyse the Cs EXAFS of the samples from the Na-CS leaching experiment. For both Na-CS samples, prior to leaching and after 20 days of leaching (#3 and 4, Fig. 5b and c) the EXAFS could be fitted with an oxygen coordination environment similar to the initial soil sample, with Cs-O scattering paths at 3.09-3.12 Å and at 3.37-3.45 Å (Table 1). Additionally, the radial distance of the Si/Al backscatterers were also similar in these samples at 4.01-4.08 Å. Conversely, the coordination number (of the Si/Al backscatterers) was lower than in the initial soil sample at 3.5 prior to leaching, which increased to 4 after 20 days of leaching (Table 1). This suggests that during gelling a fraction of Cs adsorbed to the basal surface was desorbed and either retained within the porewater or adsorbed to the silica nanoparticles surfaces. As the apparent Cs K_d values stabilized during 20 days of leaching, we assume that the leaching experiments are either at, or close to, equilibrium between the silica porewater and the supernatant. Then, if the decrease in the coordination number of the Si/Al backscatterers was solely caused by Cs desorption into the porewater, ~27% (after 20 days of leaching) of the Cs present in the Na-CS samples would reside in the porewater, equating to ~200 ppm Cs in the porewater and the supernatant. However, after 20 days only 1.9 ppm Cs was detected in the supernatant

(Fig. S1b). Furthermore, the apparent K_D value during the leaching experiment to produce samples for XAS analyses stabilized at a value ($3.6 \cdot 10^2$ ml/g) in excess of the K_D value from the parallel equilibrium desorption experiment ($1.8 \cdot 10^2$ ml/g, Fig. S1b). It is thus likely that the variation in the coordination number in both Na-CS samples resulted from Cs complexation with silica nanoparticles. Subsequently, during leaching, the decrease in the pH in the porewater to 8.6 (below the adsorption edge of Cs adsorption to amorphous silica)⁴¹ induced Cs desorption from the silica nanoparticle surfaces and a subsequent increase in the proportion of Cs complexed with the clay minerals (compared to the proportion before leaching). Interestingly, we were not able to fit Cs backscatters to the EXAFS spectra of the Na-CS samples (Table 1, Fig. 5b and c) compared to the multinuclear surface species in the colloidal silica standard (Fig. 5b and c). Previous studies have shown that a transition from mononuclear to multinuclear surface complexes occurs when increasing the metal concentration.^{20, 72} We thus suggest that, at these lower concentrations (compared to the colloidal silica standard) during the Cs leaching experiments, the interaction of Cs with the silica nanoparticles occurred through the formation of (mononuclear) outer-sphere surface complexes (Table 1, Fig. 5b and c).

Conclusions

For any environmental engineering strategy to mitigate the risks of legacy waste sites, it is essential that all impacts on the mobility of contaminants are well understood. From the presented results of a comprehensive set of leaching experiments on soil and waste materials contaminated with Sr and Cs, we have developed a conceptual model on the (competing) impacts of the (components of) colloidal silica gel on Sr and Cs geochemistry in a binary contaminated solid – colloidal silica gel system (Fig. 6). We have demonstrated that Sr and Cs interact with clayey soils through inner-sphere surface complexation to clay minerals (Sr) or at the basal surface of illite-smectite and/or kaolinite (Cs) and through incorporation into the interlayer of illite-smectite (trace Cs, Fig. 6D). Even though cations in the saline accelerant compete with Sr and Cs for adsorption sites (Fig. 3),⁵ colloidal silica gel caused an increase in the distribution coefficients compared to equilibrium desorption experiments by providing a large amount of (silica) surface area for outer-sphere Sr and Cs surface complexation (Fig. 6B, C and D), in conjunction with initial high pH values of ~ 10 (i.e. during the initial high ionic strength when competing cations from the accelerant are present). Our conceptual model thus shows that within these binary systems, colloidal silica materials not only inhibit water flow, but also significantly increase the immobilization capacity for Sr and Cs in contaminated soils (and wastes, Fig. 2). Our conceptual model could form the basis for a more quantitative (modelling) approach to predict the impacts of colloidal silica materials on the geochemistry of risk determining contaminants at the larger spatial and longer time scales

expected for the size and lifetime of environmental engineering strategies.

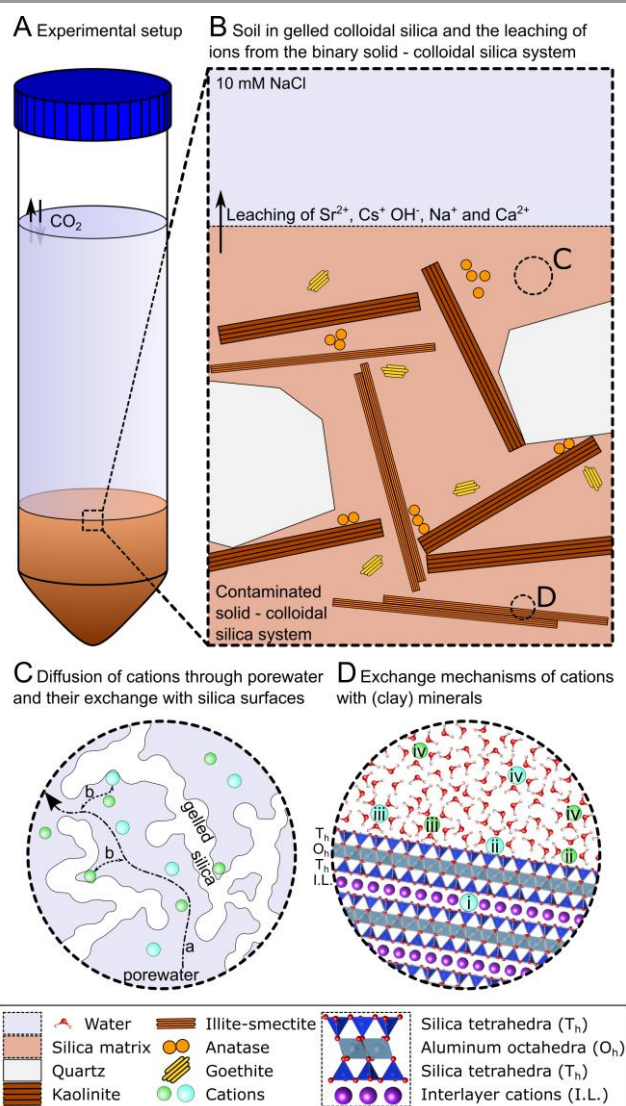


Fig. 6. Schematic representation of the conceptual model. A: The leaching experiments within 50 ml centrifuge tubes, and a representation of CO_2 exchange between the leaching solution and the headspace/atmosphere. B-D: Overview of the processes at various length scales. B: contaminated soil minerals embedded in a colloidal silica matrix (not to scale); the arrow represents leaching of ions into the supernatant (10 mM NaCl); C: (a) diffusion of cations (Sr^{2+} , Cs^+ , Na^+ and Ca^{2+}) through gelled silica nanoparticles, and (b) ad- and desorption of cations to silica surfaces; D: immobilization of Sr and Cs through interactions with (clay) minerals (using illite as an example based on the crystallographic information from Drits et al. (54). The position of the cations visualize diffusion/incorporation into the interlayer (i), the formation of inner-sphere (ii) and outer-sphere surface complexes (iii), and retention of cations within the electric diffuse layer (iv)³⁰

Overall, our conceptual model highlights that nanoparticulate colloidal silica gels have strong potential for use within risk mitigation strategies for legacy nuclear waste sites, specifically with respect to Sr and Cs, and potentially for a wider range of radionuclides, and environmental engineering strategies where the physical properties of colloidal silica gels (e.g. low viscosity, chemical inertness, and negligible toxicity) are beneficial. However, in order to fully benefit from its potential at nuclear legacy sites, we suggest that similarly comprehensive leaching

(and adsorption) studies should be performed on a wider range of potential risk determining radionuclides expected at legacy nuclear waste sites, including U, Pu and Am.^{7, 8, 10, 75}

Conflicts of interest

There are no conflicts to declare.

Acknowledgements

We would like to acknowledge Diamond Light Source for awarding us with XAS beamtime at the Core XAS beamline (B18) under grant number: SP17114. Further we would like to thank Dr Gianantonio Cibirin for his assistance during XAS beamtime. We thank Lida Mokhber Shahin and Jennifer Harrison for their assistance with the radiochemical analyses and Henri Wong for the ICP-AES analyses. Finally, we would like to thank Dr Gráinne El Mountassir for preliminary discussions on the colloidal silica materials.

References

- 1 *Geological disposal facilities for radioactive waste specific safety guide. IAEA Safety Standards Series No. SSG-14.*, IAEA, Vienna, 2011.
- 2 *Upgrading of near surface repositories for radioactive waste. Technical Report Series No. 433.*, IAEA, Vienna, 2005.
- 3 K. J. Cantrell, W. Um, B. D. Williams, M. E. Bowden, B. Gartman, W. W. Lukens, E. C. Buck and E. J. Mausolf, Chemical stabilization of Hanford tank residual waste, *Journal of Nuclear Materials*, 2014, **446**, 246-256.
- 4 N. L. Hakem, I. Al Mahamid, J. A. Apps and G. J. Moridis, Sorption of cesium and strontium on Hanford soil, *Journal of Radioanalytical and Nuclear Chemistry*, 2000, **246**, 275-278.
- 5 N. Hakem, J. A. Apps, G. J. Moridis and I. Al Mahamid, Sorption of fission product radionuclides, ¹³⁷Cs and ⁹⁰Sr, by Savannah River Site sediments impregnated with colloidal silica, *Radiochimica Acta*, 2004, **92**, 419-432.
- 6 S. H. Wallace, S. Shaw, K. Morris, J. S. Small, A. J. Fuller and I. T. Burke, Effect of groundwater pH and ionic strength on strontium sorption in aquifer sediments: Implications for ⁹⁰Sr mobility at contaminated nuclear sites, *Applied Geochemistry*, 2012, **27**, 1482-1491.
- 7 K. Morris, J. C. Butterworth and F. R. Livens, Evidence for the remobilization of Sellafield waste radionuclides in an intertidal salt marsh, West Cumbria, U.K, Estuarine, *Coastal and Shelf Science*, 2000, **51**, 613-625.
- 8 T. E. Payne, J. J. Harrison, C. E. Hughes, M. P. Johansen, S. Thiruvoth, K. L. Wilsher, D. I. Cendón, S. I. Hankin, B. Rowling and A. Zawadzki, Trench 'Bathtubbing' and surface plutonium contamination at a legacy radioactive waste site, *Environmental Science and Technology*, 2013, **47**, 13284-13293.
- 9 D. I. Cendón, C. E. Hughes, J. J. Harrison, S. I. Hankin, M. P. Johansen, T. E. Payne, H. Wong, B. Rowling, M. Vine, K. Wilsher, A. Guinea and S. Thiruvoth, Identification of sources and processes in a low-level radioactive waste site adjacent to landfills: groundwater hydrogeochemistry and isotopes, *Australian Journal of Earth Sciences*, 2015, **62**, 123-141.
- 10 A. Ikeda-Ohno, J. J. Harrison, S. Thiruvoth, K. Wilsher, H. K. Y. Wong, M. P. Johansen, T. D. Waite and T. E. Payne, Solution speciation of plutonium and americium at an Australian legacy radioactive waste disposal site, *Environmental Science and Technology*, 2014, **48**, 10045-10053.
- 11 P. M. Gallagher, S. Spatari and J. Cucura, Hybrid life cycle assessment comparison of colloidal silica and cement grouted soil barrier remediation technologies, *Journal of Hazardous Materials*, 2013, **250-251**, 421-430.
- 12 M. Pedrotti, C. Wong, G. El Mountassir and R. J. Lunn, An analytical model for the control of silica grout penetration in natural groundwater systems, *Tunnelling and Underground Space Technology*, 2017, **70**, 105-113.
- 13 C. Wong, M. Pedrotti, G. El Mountassir and R. J. Lunn, A study on the mechanical interaction between soil and colloidal silica gel for ground improvement, *Engineering Geology*, 2018, **243**, 84-100.
- 14 T. Zhang, G. V. Lowry, N. L. Capiro, J. Chen, W. Chen, Y. Chen, D. D. Dionysiou, D. W. Elliott, S. Ghoshal, T. Hofmann, H. Hsu-Kim, J. Hughes, C. Jiang, G. Jiang, C. Jing, M. Kavanaugh, Q. Li, S. Liu, J. Ma, B. Pan, T. Phenrat, X. Qu, X. Quan, N. Saleh, P. J. Vikesland, Q. Wang, P. Westerhoff, M. S. Wong, T. Xia, B. Xing, B. Yan, L. Zhang, D. Zhou and P. J. J. Alvarez, In situ remediation of subsurface contamination: Opportunities and challenges for nanotechnology and advanced materials, *Environmental Science: Nano*, 2019, **6**, 1283-1302.
- 15 X. Wang, L. Chen, L. Wang, Q. Fan, D. Pan, J. Li, F. Chi, Y. Xie, S. Yu, C. Xiao, F. Luo, J. Wang, C. Chen, W. Wu, W. Shi and S. Wang, Synthesis of novel nanomaterials and their application in efficient removal of radionuclides, *Science China Chemistry*, 2019, **62**, 933-967.
- 16 W. Cheng, C. Ding, Q. Wu, X. Wang, Y. Sun, W. Shi, T. Hayat, A. Alsaedi and Z. Chai, Mutual effect of U(VI) and Sr(II) on graphene oxides: Evidence from EXAFS and theoretical calculations, *Environmental Science: Nano*, 2017, **4**, 1124-1131.
- 17 Y. Sun, W. Song, Y. Liu, T. Hayat, A. Alsaedi, Y. Ai, V. K. Sharma and X. Wang, Mutual effect of Cs(i) and Sr(ii) sorption on nano-talc investigated by EXAFS, modeling and theoretical calculations, *Environmental Science: Nano*, 2019, **6**, 672-683.
- 18 V. Sanial, K. O. Buesseler, M. A. Charette and S. Nagao, Unexpected source of Fukushima-derived radiocesium to the coastal ocean of Japan, *Proceedings of the National Academy of Sciences of the United States of America*, 2017, **114**, 11092-11096.
- 19 C. Micheau, D. Dedovets, P. Bauduin, O. Diat and L. Girard, Nanoparticle foam flotation for caesium decontamination using a pH-sensitive surfactant, *Environmental Science: Nano*, 2019, **6**, 1576-1584.
- 20 G. E. Brown Jr, A. L. Foster and J. D. Ostergren, Mineral surfaces and bioavailability of heavy metals: A molecular-scale perspective, *Proceedings of the National Academy of Sciences of the United States of America*, 1999, **96**, 3388-3395.
- 21 A. D. Ebner, J. A. Ritter and J. D. Navratil, Adsorption of cesium, strontium, and cobalt ions on magnetite and a magnetite - Silica composite, *Industrial and Engineering Chemistry Research*, 2001, **40**, 1615-1623.
- 22 M. K. Ridley, M. L. Machesky and J. D. Kubicki, Experimental study of strontium adsorption on anatase nanoparticles as a function of size with a density functional theory and CD model interpretation, *Langmuir*, 2015, **31**, 703-713.
- 23 W. R. Bower, K. Morris, J. F. W. Mosselmans, O. R. Thompson, A. W. Banford, K. Law and R. A. D. Patrick, Characterising legacy spent nuclear fuel pond materials using microfocus X-ray absorption spectroscopy, *Journal of Hazardous Materials*, 2016, **317**, 97-107.
- 24 N. Sahai, S. A. Carroll, S. Roberts and P. A. O'Day, X-ray absorption spectroscopy of strontium(II) coordination. II. Sorption and precipitation at kaolinite, amorphous silica, and goethite surfaces, *Journal of Colloid and Interface Science*, 2000, **222**, 198-212.

- 25 A. J. Fuller, S. Shaw, C. L. Peacock, D. Trivedi and I. T. Burke, EXAFS Study of Sr sorption to illite, goethite, chlorite, and mixed sediment under hyperalkaline conditions, *Langmuir*, 2016, **32**, 2937-2946.
- 26 B. Siroux, A. Wisoq, C. Beaucaire, C. Latrille, C. Petcut, J. Calvaire, M. Tabarant, M. F. Benedetti and P. E. Reiller, Adsorption of strontium and caesium onto an Na-illite and Na-illite/Na-smectite mixtures: Implementation and application of a multi-site ion-exchange model, *Applied Geochemistry*, 2018, **99**, 65-74.
- 27 T. Missana, M. Garcia-Gutierrez and U. Alonso, Sorption of strontium onto illite/smectite mixed clays, *Physics and Chemistry of the Earth*, 2008, **33**, S156-S162.
- 28 T. H. Wang, T. E. Payne, J. J. Harrison and S. P. Teng, Interactions involving strontium and various organic acids on the surface of bentonite (MX-80), *Journal of Radioanalytical and Nuclear Chemistry*, 2015, **304**, 95-105.
- 29 R. H. Parkman, J. M. Charnock, F. R. Livens and D. J. Vaughan, A study of the interaction of strontium ions in aqueous solution with the surfaces of calcite and kaolinite, *Geochimica et Cosmochimica Acta*, 1998, **62**, 1481-1492.
- 30 G. Sposito, N. T. Skipper, R. Sutton, S. H. Park, A. K. Soper and J. A. Greathouse, Surface geochemistry of the clay minerals, *Proceedings of the National Academy of Sciences of the United States of America*, 1999, **96**, 3358-3364.
- 31 T. Missana, A. Benedicto, M. García-Gutiérrez and U. Alonso, Modeling cesium retention onto Na-, K- and Ca-smectite: Effects of ionic strength, exchange and competing cations on the determination of selectivity coefficients, *Geochimica et Cosmochimica Acta*, 2014, **128**, 266-277.
- 32 T. Missana, M. García-Gutiérrez, A. Benedicto, C. Ayora and K. De-Pourcq, Modelling of Cs sorption in natural mixed-clays and the effects of ion competition, *Applied Geochemistry*, 2014, **49**, 95-102.
- 33 M. Gutierrez and H. R. Fuentes, A mechanistic modeling of montmorillonite contamination by cesium sorption, *Applied Clay Science*, 1996, **11**, 11-24.
- 34 S. Kerisit, M. Okumura, K. M. Rosso and M. Machida, Molecular simulation of cesium adsorption at the basal surface of phyllosilicate minerals, *Clays and Clay Minerals*, 2016, **64**, 389-400.
- 35 I. F. Vasconcelos, B. A. Bunker and R. T. Cygan, Molecular dynamics modeling of ion adsorption to the basal surfaces of kaolinite, *Journal of Physical Chemistry C*, 2007, **111**, 6753-6762.
- 36 B. C. Bostick, M. A. Vairavamurthy, K. G. Karthikeyan and J. Chorover, Cesium adsorption on clay minerals: An EXAFS spectroscopic investigation, *Environmental Science and Technology*, 2002, **36**, 2670-2676.
- 37 A. J. Fuller, S. Shaw, M. B. Ward, S. J. Haigh, J. F. W. Mosselmans, C. L. Peacock, S. Stackhouse, A. J. Dent, D. Trivedi and I. T. Burke, Caesium incorporation and retention in illite interlayers, *Applied Clay Science*, 2015, **108**, 128-134.
- 38 A. J. Fuller, S. Shaw, C. L. Peacock, D. Trivedi, J. S. Small, L. G. Abrahamsen and I. T. Burke, Ionic strength and pH dependent multi-site sorption of Cs onto a micaceous aquifer sediment, *Applied Geochemistry*, 2014, **40**, 32-42.
- 39 S. A. Carroll, S. K. Roberts, L. J. Criscenti and P. A. O'Day, Surface complexation model for strontium sorption to amorphous silica and goethite, *Geochemical Transactions*, 2008, **9**.
- 40 S. Choi, P. A. O'Day, N. A. Rivera, K. T. Mueller, M. A. Vairavamurthy, S. Seraphin and J. Chorover, Strontium speciation during reaction of kaolinite with simulated tank-waste leachate: Bulk and microfocused EXAFS analysis, *Environmental Science and Technology*, 2006, **40**, 2608-2614.
- 41 S. Kumar, B. S. Tomar, S. Ramanathan and V. K. Manchanda, Effect of humic acid on cesium sorption on silica colloids, *Radiochimica Acta*, 2006, **94**, 369.
- 42 N. Tantemsapya and J. N. Meegoda, Estimation of diffusion coefficient of chromium in colloidal silica using digital photography, *Environmental Science and Technology*, 2004, **38**, 3950-3957.
- 43 K. Maher, J. R. Bargar and G. E. Brown, Environmental speciation of actinides, *Inorganic Chemistry*, 2013, **52**, 3510-3532.
- 44 A. J. Dent, G. Cibin, S. Ramos, S. A. Parry, D. Gianolio, A. D. Smith, S. M. Scott, L. Varandas, S. Patel, M. R. Pearson, L. Hudson, N. A. Krumpa, A. S. Marsch and P. E. Robbins, Performance of B18, the core EXAFS bending magnet beamline at diamond, *Journal of Physics: Conference Series*, 2013, **430**.
- 45 B. Ravel and M. Newville, ATHENA, ARTEMIS, HEPHAESTUS: data analysis for X-ray absorption spectroscopy using IFFFIT, *Journal of Synchrotron Radiation*, 2005, **12**, 537-541.
- 46 B. Ravel and J. J. Rehr, Full multiple scattering XANES calculations, *Journal De Physique. IV : JP*, 1997, **7**, C2-229-C222-230.
- 47 V. Drits, J. Srodon and D. D. Eberl, XRD measurement of mean crystalline thickness of illite and illite/smectite: Reappraisal of the Kubler index and the Scherrer equation, *Clays and Clay Minerals*, 1997, **45**, 461-475.
- 48 D. Pan, N. Zhang, C. Han, S. Yang, C. Zhang and Z. Xie, Experimental study of imbibition characteristics of silica sol in coal-measure mudstone matrix, *Applied Sciences (Switzerland)*, 2017, **7**.
- 49 L. Zhang, A. Mikhailovskaya, D. Constantin, G. Foffi, J. Tavacoli, J. Schmitt, F. Muller, C. Rochas, N. Wang, D. Langevin and A. Salonen, Varying the counter ion changes the kinetics, but not the final structure of colloidal gels, *Journal of Colloid and Interface Science*, 2016, **463**, 137-144.
- 50 R. Huang, C. Ma, Q. He, J. Ma, Z. Wu and X. Huangfu, Ion specific effects of monovalent cations on deposition kinetics of engineered nanoparticles onto the silica surface in aqueous media, *Environmental Science: Nano*, 2019, **6**, 2712-2723.
- 51 J. Škvarla, Quantitative interpretation of anomalous coagulation behavior of colloidal silica using a swellable polyelectrolyte gel model of electrical double layer, *Langmuir*, 2013, **29**, 8809-8824.
- 52 R. Mondragon, J. E. Julia, A. Barba and J. C. Jarque, Characterization of silica-water nanofluids dispersed with an ultrasound probe: A study of their physical properties and stability, *Powder Technology*, 2012, **224**, 138-146.
- 53 A. H. Jalil and U. Pyell, Quantification of zeta-potential and electrokinetic Surface charge density for colloidal silica nanoparticles dependent on type and Concentration of the counterion: Probing the outer Helmholtz plane, *Journal of Physical Chemistry C*, 2018, **122**, 4437-4453.
- 54 D. Li, M. H. Nielsen, J. R. Lee, C. Frandsen, J. F. Banfield and J. J. De Yoreo, Direction-specific interactions control crystal growth by oriented attachment, *Science*, 2012, **336**, 1014-1018.
- 55 X. M. Zang, J. M. Li, Y. Wang, Y. Y. Liu, Z. B. Wei, L. Yang and A. J. Miao, A facile method to study the bioaccumulation kinetics of amorphous silica nanoparticles by quantum dot embedding, *Environmental Science: Nano*, 2018, **5**, 2830-2841.
- 56 R. D. Shannon and C. T. Prewitt, Effective ionic radii and crystal chemistry, *Journal of Inorganic and Nuclear Chemistry*, 1970, **32**, 1427-1441.
- 57 M. L. Whittaker, L. N. Lammers, S. Carrero, B. Gilbert and J. F. Banfield, Ion exchange selectivity in clay is controlled by nanoscale chemical-mechanical coupling, *Proceedings of the*

- National Academy of Sciences of the United States of America*, 2019, **116**, 22052-22057.
- 58 X. Yin, X. Wang, H. Wu, T. Ohnuki and K. Takeshita, Enhanced desorption of cesium from collapsed interlayer regions in vermiculite by hydrothermal treatment with divalent cations, *Journal of Hazardous Materials*, 2017, **326**, 47-53.
- 59 T. Cole, G. Bidoglio, M. Soupioni, M. O'Gorman and N. Gibson, Diffusion mechanisms of multiple strontium species in clay, *Geochimica et Cosmochimica Acta*, 2000, **64**, 385-396.
- 60 S. H. Wallace, S. Shaw, K. Morris, J. S. Small and I. T. Burke, Alteration of sediments by hyperalkaline k-rich cement leachate: Implications for strontium adsorption and incorporation, *Environmental Science and Technology*, 2013, **47**, 3694-3700.
- 61 M. E. McBriarty, J. A. Soltis, S. Kerisit, O. Qafoku, M. E. Bowden, E. J. Bylaska, J. J. De Yoreo and E. S. Ilton, Trace Uranium Partitioning in a Multiphase Nano-FeOOH System, *Environmental Science and Technology*, 2017, **51**, 4970-4977.
- 62 M. E. McBriarty, S. Kerisit, E. J. Bylaska, S. Shaw, K. Morris and E. S. Ilton, Iron Vacancies Accommodate Uranyl Incorporation into Hematite, *Environmental Science and Technology*, 2018, **52**, 6282-6290.
- 63 J. A. Soltis, M. E. McBriarty, O. Qafoku, S. N. Kerisit, E. Nakouzi, J. J. De Yoreo and E. S. Ilton, Can mineral growth by oriented attachment lead to incorporation of uranium(vi) into the structure of goethite?, *Environmental Science: Nano*, 2019, **6**, 3000-3009.
- 64 J. P. R. De Villiers, Crystal structures of aragonite, strontianite, and witherite, *American Mineralogist*, 1971, **56**, 758-767.
- 65 J. Chorover, S. Choi, P. Rotenberg, R. J. Serne, N. Rivera, C. Strepka, A. Thompson, K. T. Mueller and P. A. O'Day, Silicon control of strontium and cesium partitioning in hydroxide-weathered sediments, *Geochimica et Cosmochimica Acta*, 2008, **72**, 2024-2047.
- 66 D. J. Hodkin, D. I. Stewart, J. T. Graham, G. Cibir and I. T. Burke, Enhanced crystallographic incorporation of strontium(II) ions into calcite via preferential adsorption at obtuse growth steps, *Crystal Growth and Design*, 2018, **18**, 2836-2843.
- 67 M. Nakano, K. Kawamura and Y. Ichikawa, Local structural information of Cs in smectite hydrates by means of an EXAFS study and molecular dynamics simulations, *Applied Clay Science*, 2003, **23**, 15-23.
- 68 S. M. Park, D. S. Alessi and K. Baek, Selective adsorption and irreversible fixation behavior of cesium onto 2:1 layered clay mineral: A mini review, *Journal of Hazardous Materials*, 2019, **369**, 569-576.
- 69 R. Černý, V. Favre-Nicolin and B. Bertheville, A tetragonal polymorph of caesium hydroxide monohydrate, CsOH·H₂O, from x-ray powder data, *Acta Crystallographica Section C: Crystal Structure Communications*, 2002, **58**, i31-i32.
- 70 H. Jacobs, B. Harbrecht, P. Müller and W. Bronger, Struktur und Eigenschaften von Caesiumhydroxid-monohydrat – einer Verbindung, die in ihrer Hochtemperatur-form schichtenförmige [H₃O⁺]-Polyanionen enthält [1, 2], *ZAAC - Journal of Inorganic and General Chemistry*, 1982, **491**, 154-162.
- 71 S. E. Fendorf, G. M. Lamble, M. G. Stapleton, M. J. Kelley and D. L. Sparks, Mechanisms of Chromium(III) Sorption on Silica. 1. Cr(III) Surface Structure Derived by Extended X-ray Absorption Fine Structure Spectroscopy, *Environmental Science and Technology*, 1994, **28**, 284-289.
- 72 C. J. Chisholm-Brause, P. A. O'Day, G. E. Brown Jr and G. A. Parks, Evidence for multinuclear metal-ion complexes at solid/water interfaces from X-ray absorption spectroscopy, *Nature*, 1990, **348**, 528-531.
- 73 P. A. O'day, G. E. Brown, Jr. and G. A. Parks, X-ray absorption spectroscopy of cobalt(ii) multinuclear surface complexes and surface precipitates on kaolinite, *Journal of Colloid And Interface Science*, 1994, **165**, 269-289.
- 74 Y. Li, L. Xu, P. Bai, G. Rong, D. Zhang, J. Diwu, W. Yan, Z. Chai and S. Wang, Emerging investigator series: Significantly enhanced uptake of Eu³⁺ on a nanoporous zeolitic mineral in the presence of UO₂²⁺: Insights into the impact of cation-cation interaction on the geochemical behavior of lanthanides and actinides, *Environmental Science: Nano*, 2019, **6**, 736-746.
- 75 A. B. Kersting, D. W. Efurud, D. L. Finnegan, D. J. Rokop, D. K. Smith and J. L. Thompson, Migration of plutonium in ground water at the Nevada Test Site, *Nature*, 1999, **397**, 56-59.

ARTICLE

Table of contents entry

